APATITE-(CaOH) IN THE FOSSIL BAT GUANO DEPOSIT FROM THE "DRY" CIOCLOVINA CAVE, ŞUREANU MOUNTAINS, ROMANIA

Delia-Georgeta DUMITRAŞ AND Ştefan MARINCEA[§]

Department NII, Geological Institute of Romania, 1 Caransebeş Street, Bucharest, RO–012271 Romania

Essaïd BILAL

*Département GENERIC, Centre SPIN, Ecole Nationale Supérieure des Mines de Saint Etienne,
158, Cours Fauriel, Saint Etienne, Cedex 2, F–42023, France*

Frédéric HATERT

Laboratoire de Minéralogie, Université de Liège, Sart-Tilman, Bâtiment B-18, B–4000 Liège, Belgium

Abstract

Apatite-(CaOH) is the most abundant phosphate in the deposit of fossil bat guano in the "dry" Cioclovina Cave, Şureanu Mountains, South Carpathians, Romania. Initial deposits, of both biogenic and authigenic origin, were chemically equilibrated during diagenesis. Individual crystals are tabular, roughly hexagonal, platy on (0001) and usually between 3 and 15 μm across and up to 1 μm thick. The mean indices of refraction measured for 10 representative samples are ε 1.645(2) and ω 1.653(1). The mean measured density [D_m = 3.17(2) g/cm^3] is in good agreement with the individual calculated values. The unit-cell parameters calculated as an average of 20 sets of values are a 9.436(13), c 6.868(8) Å. The mineral is Ca-deficient, carbonate- and sulfate-bearing. Less than 2.26% of the phosphate groups are protonated, and less than 4.66% are replaced by sulfate. The cumulative incorporation of other cations in the Ca sites accounts for only 0.71 to 4.07% (mean 2.07%). Both unit-cell parameters and thermal behavior are characteristic for a hydrous A-type carbonated apatite-(CaOH), with molecular H$_2$O and carbonate substituting for hydroxyl in the structural channels. The multiplicity of the bands in the infrared absorption spectrum ($3\nu_3 + 1\nu_1 + 3\nu_4 + 2\nu_2$) is consistent with a C$_6$ point symmetry of the phosphate anion. Whitlockite obtained by thermal breakdown at 1000°C is sulfate-bearing. The authigenesis of the Cioclovina apatite-(CaOH) involved a reaction between calcium carbonate from the moonmilk flows or the cave floor and phosphoric solutions derived from guano, with brushite or an X-ray amorphous phase as a precursor.

Keywords: apatite-(CaOH), physical properties, crystal chemistry, unit-cell parameters, thermal behavior, infrared absorption data, authigenesis, "dry" Cioclovina Cave, Romania.

Sommaire

L'apatite-(CaOH) est le phosphate le plus abondant du dépôt fossile de guano de chauve-souris de la grotte «sèche» de Cioclovina, monts Şureanu, Carpates Méridionales, en Roumanie. Les dépôts initiaux, d'origine aussi bien biogène qu'authigène, ont été portés à l'équilibre chimique durant la diagenèse. Les individus cristallins sont tabulaires, vaguement hexagonaux, aplatis selon (0001). En général, ils ont entre 3 et 15 μm de diamètre et une épaisseur jusqu'à 1 μm. Les indices de réfraction moyens, mesurés sur 10 échantillons représentatifs, sont ε 1.645(2) et ω 1.653(1). La densité mesurée moyenne [D_m = 3.17(2) g/cm^3] concorde bien avec les valeurs de densité calculées. Les paramètres réticulaires, obtenus comme moyenne de 20 déterminations de valeurs individuelles, sont a 9.436(13) et c 6.868(8) Å. Le minéral est déficitaire en Ca et contient du carbonate et du sulfate. Jusqu'à 2.26% des groupes phosphate sont protonés et jusqu'à 4.66% sont remplacés par des groupes sulfate. Le remplacement du Ca par d'autres cations est mineur, ne comptant que pour 0.71 à 4.07% des sites occupés normalement par Ca (2.07% en moyenne). Les paramètres de la maille, ainsi que le comportement thermique, sont caractéristiques d'une apatite-(CaOH) carbonatée de type A, contenant de l'eau moléculaire et du carbonate en tant que remplaçants de l'hydroxyle dans les tunnels structuraux. La multiplicité des bandes dans le spectre d'absorption en infrarouge ($3\nu_3 + 1\nu_1 + 3\nu_4 + 2\nu_2$) concorde avec une symétrie ponctuelle C$_6$ de l'anion phosphate. La whitlockite obtenue après la décomposition thermique à 1000°C de l'apatite-(CaOH) contient du

§ *E-mail address*: marincea@igr.ro

sulfate. Si authigène, l'apatite-(CaOH) de Cioclovina est issue des réactions entre le carbonate de calcium des coulées de "lait de lune" ou du socle de la grotte et les solutions phosphatées dérivées du guano, ayant la brushite ou des phases amorphes aux rayons X comme précurseurs.

Mots-clés: apatite-(CaOH), propriétés physiques, chimie cristalline, paramètres de maille, comportement thermique, données d'absorption infrarouge, authigenèse, grotte «sèche» de Cioclovina, Roumanie.

Introduction

Apatite-(CaOH), ideally $Ca_5(PO_4)_3(OH)$, a mineral investigated by mineralogists, crystallographers and solid-state physicists over many years, is of great interest in material science, mainly because of its use in biomedical applications (*e.g.,* bone and teeth implants). Despite the wealth of documented research on apatite-(CaOH), and its notorious abundance in the fossil bat guano deposits in the cave environment, it is perhaps surprising that there are very few reports of integrated mineralogical data on apatite-(CaOH) from caves (*e.g.*, Balenzano *et al.* 1974, Fiore & Laviano 1991).

Normally, apatite-(CaOH) from caves is carbonate-bearing. A description using a specific term like "carbonate–hydroxylapatite" is undesirable, as this is an invalid species (Burke 2008). The use of terms such as "dahlite" (*e.g.*, Diaconu & Medeşan 1975) has caused a considerable amount of confusion in the past.

As part of a wider attempt to better characterize the phosphate minerals from the type locality of ardealite (Schadler 1932), we document the occurrence and some fundamental chemical, crystallographic and physical aspects of apatite-(CaOH) from the "dry" Cioclovina Cave, in the Şureanu Mountains, Romania. Our aims are twofold: (1) to present mineralogical data on the mineral, and (2) to investigate the chemical peculiarities of apatite-(CaOH) from a "dry" cave hosting a fossil bat guano deposit, as well as the relations between apatite-(CaOH) and the other phases.

Geological Setting

The "dry" Cioclovina Cave has received considerable attention over the years (*e.g.*, Schadler 1929, 1932, Constantinescu *et al.* 1999, Marincea *et al.* 2002, Onac *et al.* 2002, 2005, Marincea & Dumitraş 2003, 2005, Onac & White 2003, Dumitraş *et al.* 2004). Descriptions of the geological setting were presented by all these authors. The cave is located in the upper basin of Luncanilor Valley, at the base of the western slope of the Şureanu Mountains, in the Southern Carpathians, at about 16 km east–southeast of the city of Haţeg. It is developed in Tithonian – Neocomian reef limestones, which form a ridge that penetrates into the Haţeg Basin.

The huge fossil guano deposit inside the cave was mined during the first half of the last century. This resulted in magnificent exposures of the phosphate layers and greatly facilitated the investigation. The phosphate association displays all the characteristics of a "dry" system, favored by a mean temperature of about 10°C, with small variations over the seasons, and a relatively low humidity (80–88%). The mined part of the cave (Fig. 1) accounts for about 800 m out of a total length of 2002.5 m known so far (Tomuş 1999).

Apatite-(CaOH) is the most abundant calcium phosphate in the fossil deposit of bat guano from Cioclovina; it makes up to 70% by volume of the phosphate mass. The mineral is most abundant near the cave floor, which is visible where the carbonate substratum was not disturbed by mining.

Apatite-(CaOH) from Cioclovina is commonly found in intimate association with quartz, illite $2M_1$, X-ray-amorphous iron sesquioxides and, in some cases, with brushite or ardealite. Apatite-(CaOH) is the earliest formed of the phosphate phases. Other associated minerals in the fossil guano deposit include taranakite, monetite, crandallite, tinsleyite, leucophosphite, variscite, francoanellite, gypsum, bassanite, calcite, vaterite, aragonite, hematite, goethite, birnessite, romanèchite, todorokite and kaolinite. Onac *et al.* (2002, 2005) and Onac & White (2003) reported the presence of some exotic mineral species, such as berlinite, burbankite, churchite, ellestadite-(Cl), foggite, paratacamite, collinsite and sampleite, but some of these species were probably misidentified (Marincea & Dumitraş 2005).

Analytical Procedures

The mineral was investigated using scanning electron microscopy (SEM), combined with energy-dispersion spectroscopy (SEM–EDS), optical study, wet-chemical analysis, wavelength-dispersive electron-microprobe analysis (EMPA), inductively coupled plasma – atomic emission spectrometry (ICP–AES), ion chromatography, X-ray powder diffraction (XRD), thermally assisted X-ray powder diffraction, thermal analysis and infrared absorption spectrometry. Most of the analytical facilities, procedures and experimental details are similar to those already described by Marincea *et al.* (2002), Marincea & Dumitraş (2003) and Dumitraş *et al.* (2004). We will focus on the techniques not previously used.

Wavelength-dispersive electron-microprobe analyses were carried out on a fully automated CAMECA SX–50 apparatus, using the same technique, standards, operating conditions and corrections as described by Marincea *et al.* (2002).
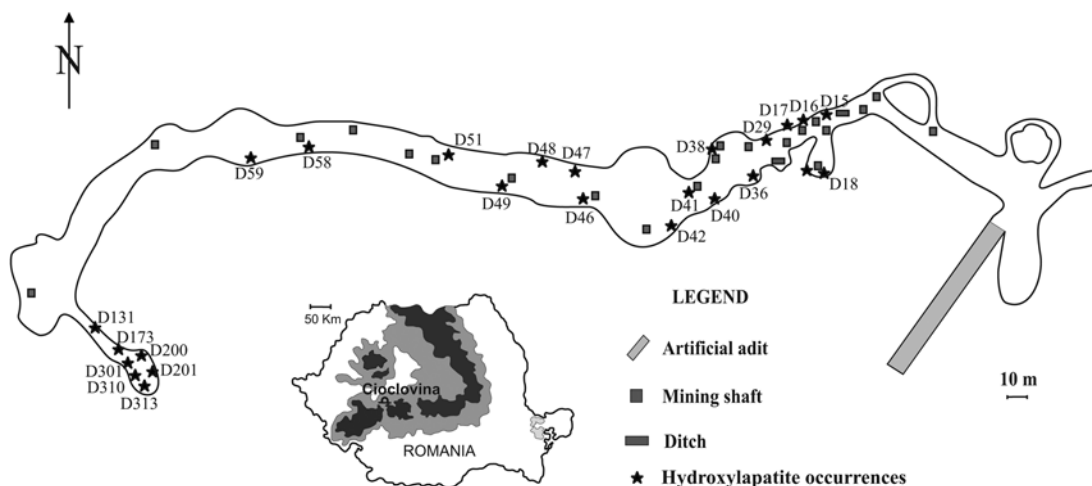
Fig. 1. Sketch of the "dry" Cioclovina Cave (the mined area) showing the location of apatite-(CaOH) samples used for this study (marked with stars). Redrawn from Constantinescu *et al.* (1999).

For all the bulk analyses, the mineral was separated by hand-picking with a preliminary screen on the basis of the mineral association in order to choose only samples devoid of brushite and ardealite. The final purity was checked by XRD. X-ray-amorphous, carbonate-bearing "moonmilk" was identified in many of the samples by infrared spectrometry.

The wet-chemical analysis was carried out on about 1 g of carefully hand-picked sample, using combined gravimetric, titrimetric and atomic absorption techniques, as described by Iosof & Neacşu (1980). The presence of S was checked by ion chromatography. The amount of CO_2 should normally be in excess because of the presence in many samples of the X-ray amorphous "moonmilk". However, a test for the CO_2 content was carried out on about 50 mg of high-purity powder tested by infrared spectrometry, using a conventional volumetric method coupled with a passage through KOH of the evolved gas, modified from that described by Shapiro & Brannock (1962).

The ICP–AES analyses were carried out following the method described by Marincea *et al.* (2002), using a Jobin–Ivon 138 Ultrace spectrometer. The sulfate anion was determined from the same solutions as used for ICP–AES analysis using a Dionex DX–500 ion chromatograph with standard AG 11–HC and AS 11–HC columns. The estimated accuracy of the analytical data is Å1% of the amount present for each of the major cations.

X-ray powder-diffraction (XRD) analysis was performed on a Siemens D–5000 Kristalloflex automated diffractometer equipped with a graphite diffracted-beam monochromator (Cu*K*α radiation, λ = 1.54056 Å). The analytical conditions were the same as described by Dumitraş *et al.* (2004). The unit-cell parameters were calculated by least-squares refinement of the XRD data, using the computer program of Appleman & Evans (1973) modified by Benoit (1987). Synthetic silicon (NBS 640b) was used as an external standard in order to verify the accuracy of the measurements.

The same operating conditions were maintained during thermally assisted diffractometry, which was carried out using a Brucker (AXS) D8 Advance diffractometer, under a constant helium flow (flow rate 20 mL/min). The powders were deposited on a stainless steel support [Ni–Cr–Fe, *a* 3.5545(5) Å at 25°C]. The heating rate was of 10°C/min, and each record was made 10 minutes after the desired temperature was attained. Three lines belonging to the support (those at ~2.05, 1.78 and 1.26 Å) were used to correct for shift of the main lines.

The thermal analysis was accomplished with a double furnace SETARAM TAG 24 thermobalance coupled with a DSC 111 thermal analyzer, with simultaneous registration of thermogravimetric (TGA), differential thermogravimetric (DTG) and differential scanning calorimetric (DSC) curves. The heating rate was 10°C/min under a constant flow of argon (flow rate 30mL/min).

The infrared absorption spectra were recorded using both a SPECORD M–80 spectrometer in the frequency range between 250 and 4000 cm^{-1} (Marincea & Dumitraş 2003), and a Fourier-transform THERMO NICOLET NEXUS spectrometer, in the frequency range between 400 and 4000 cm^{-1}. In both cases, we used standard pressed disk techniques and KBr pellets.

Luminescence tests were performed using a portable Vetter ultraviolet lamp, with 254 and 366 nm filters.

Mode of Occurrence and Morphology of Crystals

Macroscopically, apatite-(CaOH) from Cioclovina generally forms porous multilayered crusts or mamillary encrustations. The layered crusts attain 3 cm thick. They are usually deposited directly on the carbonate floor of the cave. The mineral also occurs as nodules in the fossil guano mass or in fossil bone fragments surrounded by guano. Veins of apatite-(CaOH) may also transect the fossil guano mass and locally the detrital sequences of *terra rossa* type.

Under the microscope, in transmitted light, the mineral, very fine-grained, has invariably a lamellar appearance and appears as rosette-like to radiating aggregates of tabular crystals. Individual crusts, bunches of crystals and radiating aggregates do not exceed 3 mm in thickness, and most are typically much smaller. Diffuse alteration of some apatite-(CaOH) crusts spreads out from microscopic fractures, which are marked by extremely fine veins of brushite or iron sesquioxides.

The SEM study shows that the masses macroscopically perceived as crusts are composed of randomly oriented or compact radiating aggregates of lamellar crystals, roughly hexagonal and flattened on (0001). The individual crystals are usually between 3 and 15 μm across, and up to 1 μm thick. Five modes of occurrence may be distinguished: (1) Aggregates of subspherical shape or isolated, nearly perfect spheres, generally varying in diameter between 10 and 100 μm. These aggregates (Fig. 2A) consist of very fine, densely packed radiating crystals and seem to be formed by the crystallization of an amorphous material. (2) Networks of reticulate aggregates (Fig. 2B), probably representing fragments of fossil spongy bones or other tissues. (3) Rosette-like radial aggregates with diameters up to 500 μm, built of blade-like, roughly hexagonal crystals (Fig. 2C). These could also result from the recrystallization of the initial gels and are quite common. Illite (Fig. 2D) and quartz were commonly found as inclusions in this kind of aggregate and apparently served as seeds for crystallization during the transition of an amorphous Ca phosphate toward apatite-(CaOH). (4) Aggregates of randomly oriented interlocking or subparallel platy crystals, having locally rosette-like nuclei (Fig. 2E). This kind of aggregate constitutes the major amount of the mass of layered crusts deposited directly on the carbonate substrate. (5) Aggregates of tabular hexagonal crystals intergrown on (0001), that are apparently relics of cortical ("compact") fossil bones affected by advanced recrystallization after "digestion" by the guano mass (Fig. 2F). The crystals composing these aggregates have larger dimensions (up to 100 μm across and 5 μm thick) and are the only ones to have distinguishable crystal forms: in addition to the basal pinacoid {0001}, only {1000} prisms could be identified.

Physical Properties

Some of the samples fluoresce slightly in short-wave UV light (λ = 254 nm), the response color being a light blue-violet. None of them fluoresces in long-wave (366 nm) ultraviolet radiation.

Because of the small size of the crystals, no direct measurement of the indices of refraction could be made. For this reason, they were measured on thin, platy bundles of crystals that show hexagonal peripheral faces in monochromatic light (λ = 589 nm) by immersion in Cargille oils. The values were determined as minimum and maximum values for separates from 10 selected samples (the first ten in Table 1), assuming that n_{min} = ε and n_{max} = ω. The indices of refraction obtained were ε = 1.645(2) and ω = 1.653(1), resulting in a mean index of refraction $\bar{n}$ = $(2\omega + \varepsilon)/3$ of 1.6503 for use in Gladstone–Dale calculations.

The mean density of the same representative samples of carefully hand-picked apatite-(CaOH) from Cioclovina was measured by the sink–float method at 25°C, using a mixture of methylene iodide and toluene as immersion liquid. The average of five determinations yielded D_m = 3.17(2) g/cm^3, which compares well with the calculated densities in Table 1, based on the chemical formulae (Table 2) and unit-cell parameters (Table 1), accepting Z = 1 (PDF 86–1201).

Gladstone–Dale calculations with the constants of Mandarino (1981) gave compatibility indices indicating excellent compatibilities in all cases (Table 1).

Chemical Data

Preliminary SEM–EDS analyses showed Ca and P as principal elements, with minor S, Mg, Fe, Mn, K and Na.

Results of ICP–AES analyses of 20 selected samples are presented in Table 2. The H$_2$O contents were calculated so as to fulfill charge balance, and the totals were recalculated to 100 wt.%. The amount of CO$_2$ was ignored. The formulae were normalized on the basis of 6 (S + P) and 26 (O,OH) per formula unit (*pfu*), as recommended by Fiore & Laviano (1991). This basis is appropriate for emphasizing the Ca-deficiency of our samples, which probably belong to a series of general formula Ca$_{10-x}$(HPO$_4$)$_x$(PO$_4$)$_{6-x}$(OH)$_{2-x}$, where $0 \le x \le 1$ (Berry 1967, Elliott 1994) and presumably also contain (CO$_3$)$^{2-}$ and (SO$_4$)$^{2-}$ groups.

A few remarks must be drawn on the basis of the results in Table 2: (1) No significant compositional differences occur between the various textural types of apatite-(CaOH). (2) As expected, all but six samples in Table 2 are Ca-oversaturated, showing seven-fold plus nine-fold cation totals higher than the theoretical value of 10 *apfu*. If we assume that the CO$_2$ content in each sample is 0.81 wt.%, as determined by wet-chemical analysis of the purest sample, we must consider
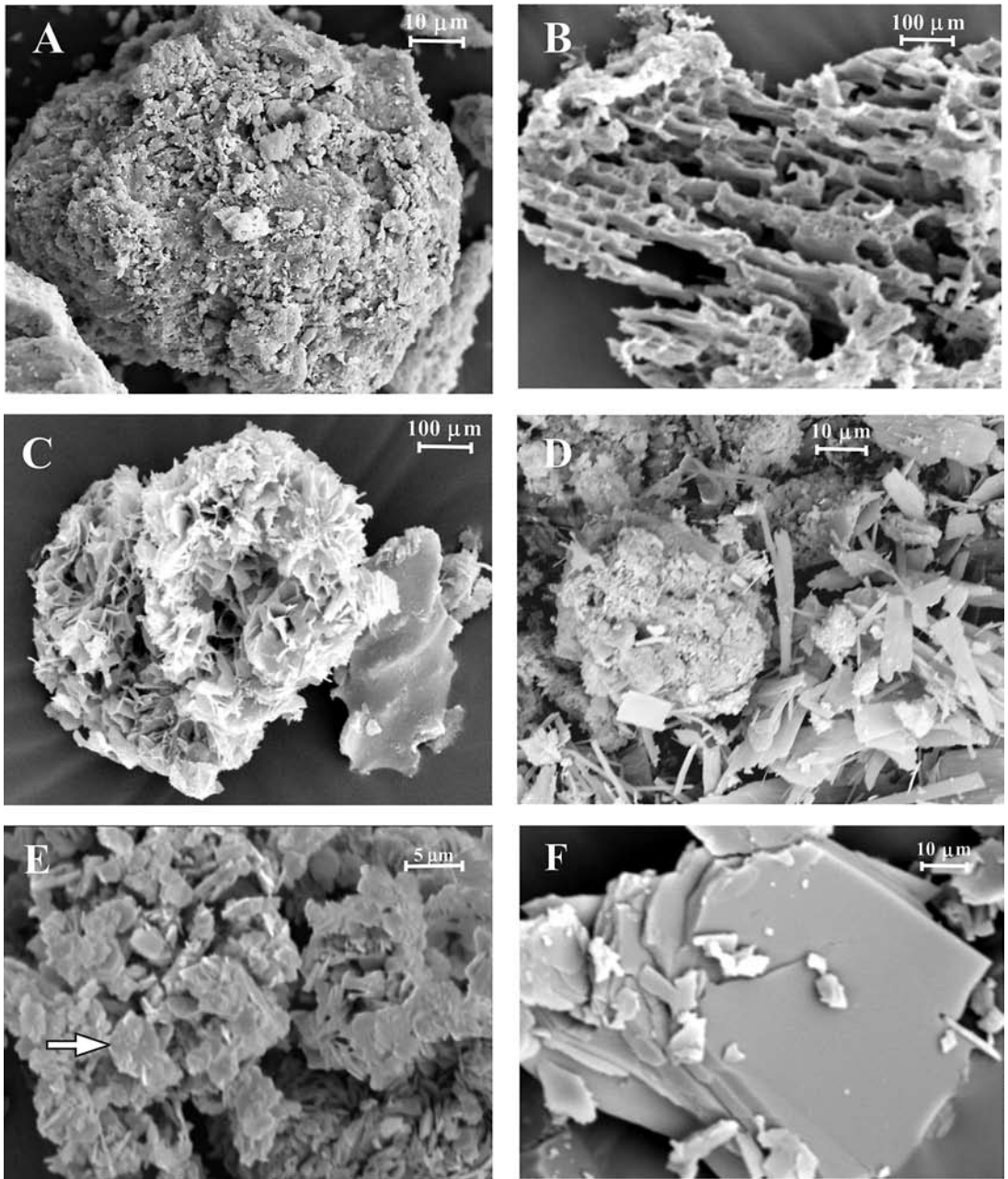
FIG. 2. SEM photomicrographs of typical aggregates of apatite-(CaOH). A. Densely packed aggregate of subspherical shape. B. Reticulate network of apatite-(CaOH) aggregates, probably a fossil fragment of spongy bone or of another tissue. C. Rosette-like radial aggregates of apatite-(CaOH). Individual crystals, roughly hexagonal, are clearly visible. D. Rosette-like aggregates of apatite-(CaOH) overgrown on platy crystals of illite. E. Aggregates of randomly oriented interlocking and subparallel platy crystals of apatite-(CaOH). The arrow indicates a perfectly shaped crystal. F. Fractured aggregate of tabular crystals of apatite-(CaOH) intergrown on (0001), representing probably a fragment of a fossil cortical bone.

TABLE 1. CRYSTALLINITY INDEX, CALCULATED UNIT-CELL AND PHYSICAL PARAMETERS
OF SELECTED SAMPLES OF APATITE-(CaOH) FROM CIOCLOVINA

Sample	C.I. [1]	a (Å)	c (Å)	V (Å^3)	M [2]	D_x [3]	K_c [4]	D'_x [5]	n_{G-D} [6]	K_p [7]	$1-(K_p/K_c)$ [8]
D 15 B	0.060	9.432(3)	6.868(3)	529.2(3)	999.889	3.136	0.2007	3.240	1.6295	0.2073	-0.0331
D 15 D	0.053	9.426(3)	6.876(4)	529.1(3)	1003.669	3.149	0.2007	3.240	1.6320	0.2065	-0.0290
D 16 A	0.047	9.435(2)	6.871(3)	529.7(3)	996.900	3.124	0.2003	3.247	1.6258	0.2082	-0.0392
D 17 A	0.042	9.441(3)	6.864(3)	529.9(3)	1002.864	3.142	0.2004	3.245	1.6296	0.2070	-0.0329
D 17 B	0.041	9.392(3)	6.872(3)	525.0(3)	1003.495	3.173	0.2007	3.240	1.6368	0.2050	-0.0212
D 18 A	0.065	9.448(3)	6.865(3)	530.7(3)	1004.265	3.141	0.2006	3.242	1.6301	0.2070	-0.0320
D 18 C	0.075	9.430(2)	6.883(3)	530.0(3)	1006.608	3.153	0.2001	3.250	1.6309	0.2063	-0.0308
D 18 D	0.038	9.439(3)	6.882(3)	531.0(3)	1002.615	3.134	0.2009	3.237	1.6297	0.2075	-0.0327
D 29 A	0.038	9.427(1)	6.864(2)	528.3(2)	1004.635	3.157	0.2008	3.239	1.6339	0.2060	-0.0259
D 29 B	0.057	9.441(3)	6.877(3)	530.8(4)	1005.713	3.145	0.2004	3.245	1.6303	0.2068	-0.0317
D 36 A	0.037	9.454(2)	6.875(2)	532.1(2)	1011.016	3.154	0.2003	3.247	1.6318	0.2062	-0.0293
D 38 C	0.063	9.437(3)	6.856(4)	528.8(4)	1006.528	3.160	0.2004	3.245	1.6332	0.2058	-0.0270
D 40 B	0.037	9.436(2)	6.861(3)	529.0(3)	1006.785	3.159	0.2006	3.242	1.6338	0.2058	-0.0261
D 41 D	0.059	9.424(3)	6.870(3)	528.4(3)	1005.958	3.160	0.2006	3.242	1.6340	0.2058	-0.0258
D 42 A	0.059	9.451(3)	6.864(3)	530.9(3)	1006.522	3.147	0.2006	3.242	1.6313	0.2066	-0.0301
D 46 B	0.067	9.449(2)	6.857(2)	530.1(3)	1006.180	3.151	0.2006	3.242	1.6321	0.2064	-0.0289
D 47 A	0.051	9.440(3)	6.867(2)	529.9(3)	1005.569	3.150	0.2004	3.245	1.6313	0.2064	-0.0301
D 49 C	0.067	9.450(3)	6.857(3)	530.2(3)	1005.468	3.148	0.2003	3.247	1.6305	0.2066	-0.0313
D 51 B	0.043	9.437(2)	6.870(2)	529.8(2)	1005.886	3.152	0.2006	3.242	1.6322	0.2063	-0.0286
D 59 A	0.041	9.433(3)	6.859(3)	528.9(3)	1004.476	3.153	0.2002	3.248	1.6312	0.2063	-0.0303

(1) crystallinity index according to Simpson (1964); (2) molecular mass; (3) calculated density; (4) chemical molar refractivity; (5) density calculated according to the Gladstone–Dale law, using the mean index of refraction ($\bar{n}$ = 1.6503), and the chemical molar refractivity; (6) $\bar{n}_x = D_x \cdot K_c + 1$; (7) physical molar refractivity, $K_P = (\bar{n} - 1)/D_x$; (8) compatibility index according to Mandarino (1981).

that part of the Ca (about 0.02 *apfu* in equivalent) is consumed for charge-balancing carbonate. In this case, all our samples are in reality Ca-deficient, which suggests that $(HPO_4)^{2-}$ groups partially replace $(PO_4)^{3-}$. However, apatite-(CaOH) samples in Table 2 contain less than 2.26% of the protonated phosphate groups, the maximum value being recorded in Sample D 18 D. (3) Sulfate groups, already reported in apatite-(CaOH) from caves (*e.g.*, Fiore & Laviano 1991), also substitute for phosphate in apatite-(CaOH) from Cioclovina: S accounts for 0.32% to 4.66% of the tetrahedral sites normally occupied by P. Consequently, we could imagine that coupled substitutions such as $(PO_4)^{3-}$ + $(OH)^- \rightarrow (SO_4)^{2-} + O^{2-}$ or $(PO_4)^{3-} + (OH)^- \rightarrow (SO_4)^{2-} + (CO_3)^{2-}$ play an important role. (4) The substitutions in the cation sites normally occupied by Ca are less important. The main substitution is Na-for-Ca, but the cumulative substitution in these sites accounts for only 0.71 to 4.07% (mean 2.07%). Other potential cations substituting for Ca were evaluated with the ICP–AES results, but were found as minor elements, as shown by the results in Table 3.

As in the case of brushite (Dumitraş *et al.* 2004), apatite-(CaOH) from Cioclovina contains less Ba than Sr, which is quite normal in apatite-(CaOH) in fossil bone [see Trueman & Tuross (2002) and refer-ences therein], but also encountered in the authigenic samples. The REE contents are relatively low. On the basis of results of partial analyses in Table 3, we can state that apatite-(CaOH) from Cioclovina is enriched in the light REE relative to the heavy REE + Y; all but three samples respect this rule, which also parallels the behavior of brushite (Dumitraş *et al.* 2004). In addition to these elements, trace concentrations of some transitional metals (*i.e.*, Cu, V, Cr and Ni) were also identified. The higher concentration of these elements in two of the analyzed samples (D 36A and D 38C B), is probably due to admixed X-ray amorphous phases and correlates with higher contents of manganese and iron.

Attempts to check the accuracy of the conclusions drawn from the results of bulk ICP–AES analyses were done using EMPA. We chose for study a fragment of fossil bone engulfed in the guano mass, which consists of pure apatite-(CaOH). Representative results for this sample (D 40 A, equivalent of D 40 B in Table 2) are summarized in Table 4. All iron was considered to be divalent, and the amount of H_2O was calculated to fulfill charge-balance conditions. A parallel wet-chemical analysis was carried out on the same sample (Table 4). A few conclusions may be drawn: (1) The proportions of halogens in the EMP analyses are probably over-

TABLE 2. CHEMICAL COMPOSITION OF SELECTED SAMPLES OF APATITE-(CaOH) FROM CIOCLOVINA

Sample	D 15B	D 15D	D 16A	D 17A	D 17B	D 18A	D 18C	D 18D	D 29A	D 29B	D 36A	D 38C	D 40B	D 41D	D 42A	D 46B	D 47A	D 49C	D 51B	D 59A
K_2O wt%	0.20	0.11	0.16	0.22	0.07	0.09	0.23	0.15	0.05	0.14	0.35	0.08	0.10	0.09	0.13	0.13	0.10	0.11	0.09	0.13
Na_2O	0.33	0.25	0.32	0.40	0.18	0.23	0.47	0.40	0.14	0.27	0.31	0.22	0.42	0.38	0.49	0.32	0.27	0.32	0.32	0.35
CaO	54.54	54.87	54.97	54.36	55.33	55.26	54.96	54.74	55.56	54.95	54.01	55.10	55.09	55.02	54.91	54.62	54.69	54.86	55.09	54.75
FeO	0.06	0.43	0.20	0.40	0.05	0.10	0.29	0.18	0.02	0.29	0.61	0.18	0.10	0.11	0.09	0.38	0.27	0.05	0.13	0.11
MnO	0.00	0.06	0.03	0.03	0.01	0.03	0.01	0.05	0.05	0.14	0.76	0.29	0.13	0.24	0.09	0.38	0.44	0.42	0.20	0.36
MgO	0.24	0.11	0.13	0.09	0.06	0.06	0.11	0.08	0.02	0.05	0.17	0.06	0.02	0.04	0.06	0.10	0.05	0.06	0.05	0.05
P_2O_5	41.38	42.06	40.48	40.59	41.67	41.42	40.47	42.33	42.12	40.80	41.72	41.02	41.63	41.84	41.99	41.85	40.87	40.66	41.72	40.51
SO_3 [1]	1.36	0.33	2.13	2.11	0.86	1.10	1.99	0.15	0.28	1.74	0.45	1.45	0.80	0.55	0.36	0.53	1.66	1.91	0.69	2.11
H_2O [2]	1.89	1.78	1.58	1.74	1.77	1.71	1.47	1.92	1.76	1.62	1.62	1.60	1.71	1.73	1.73	1.75	1.65	1.61	1.71	1.63
Total [3]	100.00	100.00	100.00	100.00	100.00	100.00	100.00	100.00	100.00	100.00	100.00	100.00	100.00	100.00	100.00	100.00	100.00	100.00	100.00	100.00
K *apfu*	0.042	0.023	0.034	0.047	0.015	0.019	0.049	0.032	0.011	0.030	0.075	0.017	0.021	0.019	0.028	0.028	0.021	0.023	0.019	0.028
Na	0.106	0.081	0.104	0.129	0.058	0.075	0.153	0.129	0.045	0.088	0.101	0.071	0.136	0.123	0.159	0.104	0.088	0.104	0.104	0.113
Ca	9.725	9.838	9.852	9.721	9.901	9.898	9.881	9.789	9.958	9.854	9.737	9.890	9.880	9.870	9.855	9.800	9.808	9.836	9.882	9.810
Fe^{2+}	0.008	0.060	0.028	0.056	0.007	0.014	0.041	0.025	0.003	0.041	0.086	0.025	0.014	0.015	0.013	0.053	0.038	0.007	0.018	0.015
Mn^{2+}	0.000	0.009	0.004	0.013	0.001	0.004	0.001	0.007	0.007	0.020	0.108	0.041	0.018	0.034	0.034	0.045	0.062	0.060	0.028	0.051
Mg	0.060	0.027	0.032	0.022	0.015	0.015	0.028	0.020	0.005	0.012	0.043	0.015	0.005	0.010	0.015	0.025	0.012	0.015	0.012	0.012
P^{5+}	5.830	5.959	5.733	5.736	5.892	5.862	5.749	5.981	5.965	5.781	5.943	5.818	5.899	5.931	5.955	5.933	5.791	5.760	5.913	5.735
S^{6+}	0.170	0.041	0.267	0.264	0.108	0.138	0.251	0.019	0.035	0.219	0.057	0.182	0.101	0.069	0.045	0.067	0.209	0.240	0.087	0.265
$(OH)^-$	2.098	1.987	1.763	1.937	1.972	1.907	1.645	2.138	1.964	1.809	1.818	1.788	1.909	1.932	1.933	1.955	1.842	1.797	1.910	1.818

(1) determined by ion chromatography; (2) as calculated to fulfill the charge balance; (3) totals recalculated at 100 wt.%. These compositions were obtained by ICP–AES analysis. The number of ions is calculated on the basis of 6 (P + S) and 26 (O,OH) atoms per formula unit (*apfu*).

TABLE 3. TRACE-ELEMENT CONTENTS OF SELECTED SAMPLES
OF APATITE-(CaOH) FROM CIOCLOVINA

Sample	Sr	Ba	Cu	V	Cr	Ni	La	Ce	Eu	Y	Yb
D 15 B	29	6.32	8.5	2.58	1.2	1.4	0.14	2.43	0.10	0.28	b.d.l.*
D 15 D	60	16.40	26.0	3.51	4.2	6.3	3.32	4.52	0.23	3.71	0.12
D 16 A	85	14.90	20.0	3.68	4.5	4.5	2.58	3.24	0.07	4.04	0.14
D 17 A	38	10.50	11.0	2.49	2.9	3.4	1.88	3.29	0.07	1.83	0.04
D 17 B	112	38.00	21.0	3.33	4.3	3.0	1.16	2.47	0.07	0.54	0.03
D 18 A	109	40.80	25.0	6.03	5.1	4.9	1.48	2.11	0.19	0.88	0.01
D 18 C	44	19.80	9.8	2.16	1.7	1.5	0.41	2.43	0.10	0.14	0.04
D 18 D	49	17.40	13.0	3.48	1.9	2.2	0.54	2.43	0.23	0.44	b.d.l.*
D 29 A	49	7.34	16.0	3.16	4.3	4.0	1.04	1.67	0.11	1.18	0.04
D 29 B	51	18.20	22.0	3.51	6.3	7.9	5.92	2.53	0.15	6.52	0.22
D 36 A	182	9.34	64.0	24.50	10.0	100.0	12.00	6.89	0.36	19.10	0.76
D 38 C	142	6.89	98.0	18.70	5.6	64.0	1.33	2.26	0.19	2.53	0.13
D 40 B	89	11.30	22.0	6.91	4.1	6.9	7.74	4.58	0.23	11.60	0.40
D 41 D	72	4.76	17.0	4.88	3.9	21.0	5.51	0.83	0.23	6.38	0.23
D 42 A	87	12.00	16.0	3.56	5.5	21.0	1.37	1.56	0.14	1.37	0.01
D 46 B	60	6.28	15.0	5.90	4.4	26.0	5.03	1.69	0.19	6.92	0.28
D 47 A	78	5.27	37.0	7.72	6.8	49.0	17.30	6.25	0.38	22.30	0.88
D 49 C	57	3.92	23.0	5.78	4.1	24.0	5.03	1.27	0.15	4.61	0.12
D 51 B	79	4.20	16.0	6.83	4.1	16.0	6.85	2.50	0.27	7.99	0.28
D 59 A	52	4.37	18.0	5.52	3.4	23.0	4.32	1.25	0.11	4.84	0.15

Concentrations are expressed in ppm. * below the detection limit. The detection limits were 0.01 ppm for Ba, V, La, Ce, Eu, Y and Yb, 0.1 ppm for Cu, Cr and Ni, and 1 ppm for Sr.

estimated owing to analytical interferences with the araldite used for fixing the samples on the support; it does not seem possible that fluorine and chlorine occupy up to 34.77% and 6.44%, respectively, of the positions normally occupied by hydroxyl, even if the analyzed apatite-(CaOH) represents a bone fragment. The wet-chemical data in Table 4 seem more accurate on this point. (2) EMP analyses reveal insignificant variations in composition among different micromounts. (3) The chemical peculiarities established by ICP–AES analyses are confirmed: up to 2.32% of the tetrahedral positions are occupied by sulfur, and the incorporation of Na, K, Mn, Fe, Mg in the *Ca* sites is minor, summing up to 2.11%. (4) Because the EMP analysis does not offer any indication for the incorporation of $(CO_3)^{2-}$ into the apatite-(CaOH) lattice, it is difficult to evaluate the deficiency in Ca of the analyzed sample; accepting, however, a CO_2 content of 0.81 wt.% as determined by wet-chemical analysis, all but one EMP dataset in Table 4 are representative of Ca-deficient apatite-(CaOH).

X-Ray Powder Data

X-ray powder diffractometry was carried out on about 100 powders of apatite-(CaOH) from Cioclovina in order to refine the cell parameters. The primary patterns are available upon request from the first author. The index of crystallinity calculated by the method recommended by Simpson (1964), involving the ratio between the total width of the diffraction peaks (211) and (112) at their half height and the greatest height of the two peaks, vary between 0.037 and 0.158. The

TABLE 4. COMPARATIVE ELECTRON-MICROPROBE AND WET-CHEMICAL ANALYTICAL DATA FOR A SELECTED SAMPLE OF APATITE-(CaOH) FROM CIOCLOVINA

Sample n [3]	D40 A[1] -	D40a[2] 6	D40b[2] 5	D40c[2] 4	D40d[2] 5	D40e[2] 5	D40f[2] 5	D40g[2] 4
K_2O wt%	0.05	0.04	0.09	0.06	0.05	0.03	0.04	0.02
Na_2O	0.30	0.23	0.27	0.27	0.10	0.20	0.15	0.17
CaO	55.10	51.15	52.44	53.13	55.04	54.11	54.89	53.31
FeO [4]	0.00	0.55	0.20	0.09	0.29	0.48	0.20	0.16
MnO	0.19	0.18	0.15	0.03	0.11	0.11	0.12	0.19
MgO	0.04	0.05	0.08	0.05	0.04	0.01	0.01	0.03
CO_2	0.81	-	-	-	-	-	-	-
P_2O_5	42.36	42.52	42.02	41.69	41.44	41.16	41.45	41.51
SO_3	-	0.99	1.03	1.11	0.67	0.91	0.75	1.11
H_2O [5]	1.80	2.77	2.21	1.96	1.21	1.08	1.16	1.91
F	0.21	1.27	1.24	1.19	0.75	1.34	1.19	0.65
Cl	0.02	0.00	0.00	0.00	0.31	0.44	0.08	0.60
O = F	-0.09	-0.54	-0.52	-0.50	-0.32	-0.57	-0.50	-0.27
O = Cl	0.00	0.00	0.00	0.00	-0.07	-0.10	-0.02	-0.14
Total	100.79	99.21	99.21	99.08	99.62	99.21	99.52	99.25
K *apfu*	0.011	0.008	0.019	0.013	0.011	0.006	0.009	0.004
Na	0.097	0.073	0.086	0.087	0.033	0.065	0.049	0.055
Ca	9.877	8.950	9.275	9.454	9.943	9.791	9.897	9.526
Fe^{2+}	0.000	0.075	0.028	0.013	0.041	0.068	0.028	0.022
Mn	0.027	0.025	0.021	0.004	0.016	0.016	0.017	0.027
Mg	0.010	0.012	0.020	0.012	0.010	0.003	0.003	0.007
C^{4+}	0.185	-	-	-	-	-	-	-
P^{5+}	6.000	5.879	5.872	5.862	5.915	5.885	5.905	5.861
S^{6+}	-	0.121	0.128	0.138	0.085	0.115	0.095	0.139
(OH)-	1.207	3.017	2.433	2.171	1.361	1.217	1.302	2.125
F	0.111	0.656	0.647	0.625	0.400	0.716	0.633	0.343
Cl	0.006	-	-	-	0.089	0.126	0.023	0.170
H_2O	0.401	-	-	-	-	-	-	-

(1) wet-chemical analysis; (2) EMP analysis; (3) number of point analyses on the same micromount; (4) all iron was considered in divalent state of oxidation; (5) as calculated for fulfillment of the charge balance. The number of ions is calculated on the basis of 6 (P+S) and 26 (O,OH,F,Cl) atoms per formula unit (*apfu*).

indices of crystallinity of the samples whose chemical compositions are given in Table 2 are reported in Table 1. Only about 12% of the analyzed samples have high indices of crystallinity, indicating that as a whole they are poorly crystalline (Simpson 1964). The unit-cell parameters were successfully refined based on a hexagonal $P6_3/m$ cell, after indexing the patterns in analogy with PDF 86–1199, 86–1201 and 86–1203. Sets of 36 to 60 reflections in the 2θ range between 10 and 70° (CuKα, λ = 1.54056 Å) for which unambiguous indexing was possible were used to refine the cell dimensions of 20 representative samples, which are summarized in Table 1. The unit-cell parameters calculated as an average of these 20 datasets of values are a 9.436(13), and c 6.868(8) Å, where the errors in the brackets correspond to the standard deviations of the mean (2σ) for each set of data. These values, as well as the individual values in Table 1, and particularly c, differ significantly from those determined by various authors for synthetic apatite-(CaOH) of stoichiometric composition [$e.g.$, a = 9.4176(5), c 6.8814(5) Å according to Elliott (1994), a 9.421(2), c 6.882(2) Å according to Brunet $et\ al$. (1999), and a 9.4302(5), c 6.8911(2) Å according to Dorozkhin & Epple (2002)].

The unit-cell dimensions of carbonate-bearing apatite-(CaOH) depend, to a first approximation, on the incorporation of $(CO_3)^{2-}$ in the structure (Elliott 1994). From this point of view, our samples generally behave like the A-type carbonated apatite-(CaOH); they are characterized by increased a unit-cell parameters due to carbonate substituting for hydroxyl group in the structural channels (Elliott 1994). The presence of carbonate in the analyzed samples could explain why the c value, 6.867(5) Å, does not differ significantly from that determined by Neweseley (1963) for a synthetic "carbonate–hydroxylapatite". As apatite-(CaOH) samples from Cioclovina have uniformly low chlorine and fluorine contents, the occupancy by halogens of the X sites in the structure (notation after Hughes $et\ al$. 1989, and Brunet $et\ al$. 1999), could not explain the change in lattice parameters.

THERMAL DECOMPOSITION

The differential thermal analysis and differential thermogravimetric curves of apatite-(CaOH) are generally smooth and featureless until 1000°C, in spite of the losses of H_2O and CO_2 recorded on the thermogravimetric curve (Fiore & Laviano 1991, Ivanova $et\ al$. 2001). This was the reason for recording the thermal curves of apatite-(CaOH) from Cioclovina using a DSC–TG–TGA coupling, in spite of the lower limits of working temperature (up to 600°C). The thermal curves recorded for a representative sample of authigenic apatite-(CaOH) from Cioclovina (D 301) are given in Figure 3. On the basis of previous studies on the thermal decomposition of the Ca-deficient carbonated apatite-(CaOH) (Elliott 1994, Ivanova $et\ al$. 2001),

we can presume that the main effects on the DTG and DSC curves are due to the following causes: (1) the loss of surface-bound H_2O (–1.43 wt.% on the TGA curve), marked by an endothermic effect at ~97°C, (2) the loss of channel H_2O (–3.61 wt.% cumulative on the TGA curve), marked by a small endothermic effect at ~198°C, and (3) the start of the carbonate migration (see below), marked by a small endothermic effect on the DTG curve at ~520°C, accompanied by an exothermic effect on the DSC curve. The loss of the lattice H_2O is continuous, whereas the loss of carbonate starts after 520°C. The TGA curve gradually declines, the total loss-in-weight at 600°C being of 6.62 wt.%.
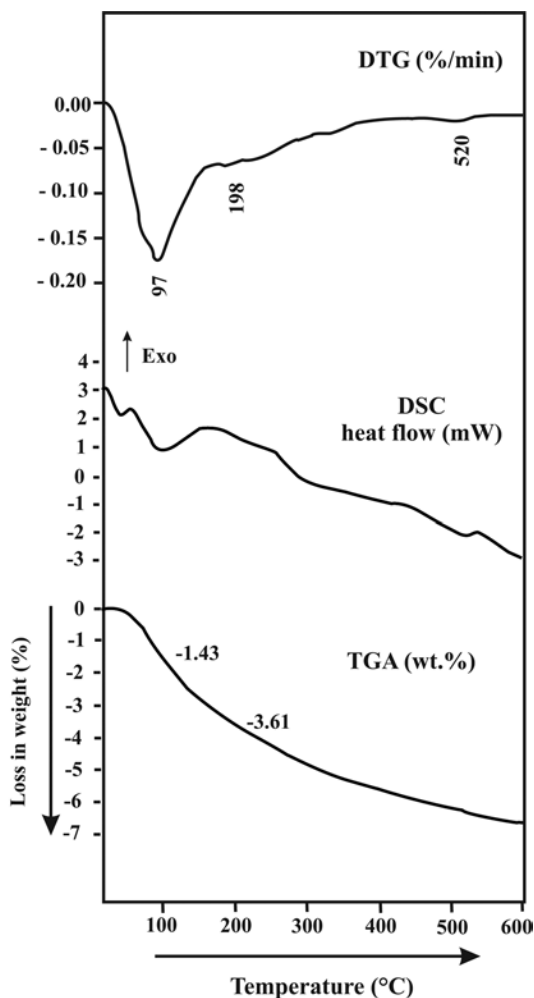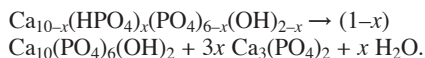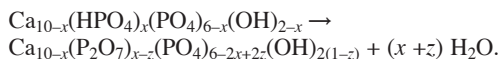

FIG. 3. Thermal curves recorded for a apatite-(CaOH) sample from Cioclovina: differential thermogravimetric (top), differential scanning calorimetric (middle) and thermogravimetric (bottom).

An XRD study of the breakdown product at 600°C, after cooling, reveals that only a phase with the apatite-(CaOH) pattern persists, without any supplementary crystalline associated phase. According to Brunet *et al*. (1999), the breakdown of Ca-deficient apatite-(CaOH) at high temperature must, however, result in the growth of β-$Ca_3(PO_4)_2$ according to the reaction:

$$Ca_{10-x}(HPO_4)_x(PO_4)_{6-x}(OH)_{2-x} \rightarrow (1-x)$$
$$Ca_{10}(PO_4)_6(OH)_2 + 3x\ Ca_3(PO_4)_2 + x\ H_2O.$$

In fact, no traces of a $Ca_3(PO_4)_2$ phase were detected, even after heating of many selected powdered samples of apatite-(CaOH) from Cioclovina at 600°C in a resistance furnace; these were held at this temperature for 24 hours in order to favor the loss of H_2O, then cooled down to 25°C. The breakdown products, analyzed by XRD, gave patterns similar with those of the starting materials. This finding apparently disagrees with our results indicating a substantial loss of H_2O, with the results of Berry (1967), which indicate the dehydration of Ca-deficient apatite-(CaOH) at 600°C, and also with the results of the thermal expansion measurements of Brunet *et al*. (1999), which indicate a breakdown at about 550°C. In fact, it is more reasonable to accept that the loss of H_2O due to the breakdown of the protonated phosphate in our sample can be explained by another reaction, proposed by Mortier *et al*. (1989):

$$Ca_{10-x}(HPO_4)_x(PO_4)_{6-x}(OH)_{2-x} \rightarrow$$
$$Ca_{10-x}(P_2O_7)_{x-z}(PO_4)_{6-2x+2z}(OH)_{2(1-z)} + (x+z)\ H_2O.$$

A weak and broad band centered at ~735 cm^{-1} in the FTIR spectra of the heated samples (not given, but available upon request from the first author) can be assigned to $(P_2O_7)^{4-}$ groups, indicating the polymerization of some of the structural orthophosphate groups, without structural breakdown.

As proven by the differential weighting, the mass loss continues until 1000°C, involving a continuous dehydration and the expelling of carbonate: the total loss in mass of sample D 301 heated to 1000°C is 7.43 wt.%. X-ray-assisted heating of this sample shows, however, that a phase with a apatite-(CaOH) pattern still persist at 900°C, allowing the refinement of its unit-cell parameters (Fig. 4, Table 5). Taking into account the dehydration, this phase must be an "oxyapatite", whose crystal structure is identical with that of apatite-(CaOH) (Alberius-Henning *et al*. 1999), generating a similar XRD pattern (PDF 01–089–6495). This inference agrees with the hypothesis that by heating the (OH)$^-$ ions in the apatite-(CaOH), anion channels are replaced by O^{2-} through the scheme 2 (OH)$^- \rightarrow$ O^{2-} + $\square$, where $\square$ is a vacancy, without any disruption of other structural constituents (Alberius-Henning *et al*. 1999).

As expected, and in agreement with experimental studies on Ca-deficient carbonated apatite-(CaOH) (Ivanova *et al*. 2001) and with studies of the thermal expansion of stoichiometric apatite-(CaOH) (Brunet *et al*. 1999), both a and c unit-cell parameters generally define an increasing trend with increasing temperature (Table 5). Two contractions of the cell can be observed, however: (1) at up to 250°C, owing to the loss of the channel H_2O, and (2) at 550–600°C, owing to the loss of carbonate (*cf*. Ivanova *et al*. 2001). The increase of a and the striking decrease of c between 600 and 650°C agree with the changes in the location of $(CO_3)^{2-}$ from $(OH)^-$ to $(PO_4)^{3-}$ sites, in a process contrary to that inferred by Ivanova *et al*. (2001) in the B-type carbonated apatite-(CaOH).

Whitlockite occurs as breakdown product at 700°C, the transformation being complete at 1000°C. The resulting whitlockite [a 10.438(8), c 37.51(7) Å at 1000°C and a 10.430(6), c 37.47(7) Å after cooling at 25°C] is, as proven by ion chromatography, sulfate-bearing, indicating that sulfate was not (entirely) expelled at 1000°C.

INFRARED ABSORPTION DATA

Figure 5 displays the infrared absorption spectra obtained for two representative samples of apatite-(CaOH) from Cioclovina with and without a Fourier-transform spectrometer, whereas Table 6 gives the wavenumbers, characters and intensities of the infrared absorption bands as well as attempts to assign the bands on the basis of the works of Baddiel & Berry (1966), Bhatnagar (1968), LeGeros *et al*. (1970) and Fowler (1973). The positions of the bands in Table 6 were established as the mean of the wavenumbers recorded for similar bands in five (IR) and, respectively, nine (FTIR) different spectra of representative samples, with standard deviations given in brackets. The primary records are available on request from the first author. As the band assignment is generally agreed upon, only the following remarks are considered important:

(1) Although both the mineral powder and the KBr were previously stored in a desiccator, both IR and FTIR spectra clearly show absorption bands due to

TABLE 5. EVOLUTION OF THE UNIT-CELL PARAMETERS OF THE CIOCLOVINA APATITE-(CaOH) WITH HEATING*

T (°C)	a (Å)	c (Å)	V (Å^3)	n [1]	N [2]
25	9.433(2)	6.874(3)	529.7(3)	3	45
250	9.420(3)	6.862(3)	527.4(3)	6	40
500	9.421(4)	6.887(4)	529.4(4)	7	47
550	9.449(4)	6.898(6)	533.4(5)	9	35
600	9.419(4)	6.879(6)	528.6(5)	10	33
650	9.447(4)	6.859(5)	530.2(4)	10	35
700	9.448(3)	6.878(3)	531.7(4)	3	27
800	9.459(4)	6.878(5)	532.9(5)	3	27
900	9.471(6)	6.881(7)	534.5(6)	4	22

* determined by least-squares refinement of 50 reflections in the 2θ range 10–90°; (1) number of least-squares refining cycles; (2) number of unrejected reflections used for refinement.
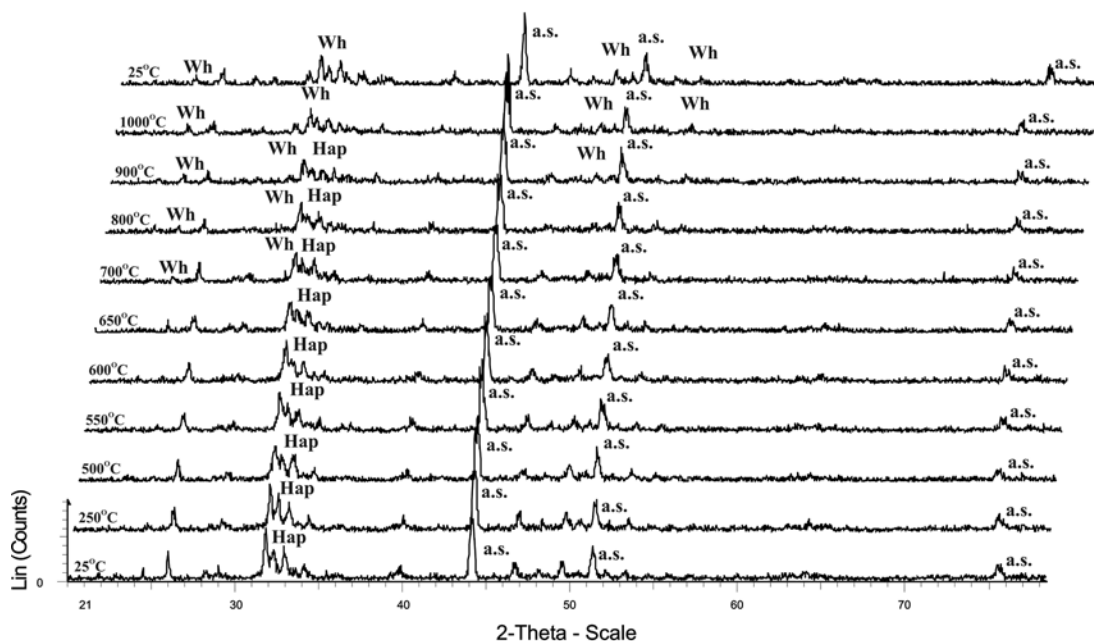
FIG. 4.   X-ray powder patterns of a representative sample of apatite-(CaOH) from Cioclovina, as a function of temperature. Representative lines of austenitic steel (a.s.), whitlockite (Wh) and apatite-(CaOH) (Hap) are marked on the figure.

TABLE 6. POSITIONS AND ASSIGNMENTS OF THE INFRARED ABSORPTION BANDS RECORDED FOR SELECTED SAMPLES OF APATITE-(CaOH) FROM CIOCLOVINA [1]

Structural group	Vibrational mode	Wavenumber (cm^{-1})		Character, intensity [2]
		IR	FTIR	
(OH)$^-$	stretching	3576(2)	3570(1)	sh (shd), w
H$_2$O [3]	H-O-H stretching	3407(2)	3402(2)	b, m
H$_2$O [3]	H-O-H "scissors" bending	1633(3)	1631(2)	b, m
(CO$_3$)$^{2-}$ [4]	ν_3 antisymmetric stretching	1457(1)	1456(1)	b, m
(CO$_3$)$^{2-}$ [4]	ν_3' antisymmetric stretching	1420(1)	1420(1)	b, m
(PO$_4$)$^{3-}$	ν_3 antisymmetric stretching	1093(2)	1095(1)	sh, vs
(PO$_4$)$^{3-}$	ν_3' antisymmetric stretching	1064(2)	1062(2)	shd, vs
(PO$_4$)$^{3-}$	ν_3'' antisymmetric stretching	1037(2)	1035(1)	b, vs
(PO$_4$)$^{3-}$	ν_1 symmetric stretching	961(4)	961(1)	sh, w
(CO$_3$)$^{2-}$ [4]	ν_2 out-of-plane bending (O-C-O)	873(1)	873(1)	sh, m
(OH)$^-$	OH libration	635(1)	635(1)	b (shd), w
(PO$_4$)$^{3-}$	ν_4 in-plane bending (O-P-O)	603(1)	602(1)	sh, s
(PO$_4$)$^{3-}$	ν_4' in-plane bending (O-P-O)	574(1)	574(1)	shd, s
(PO$_4$)$^{3-}$	ν_4'' in-plane bending (O-P-O)	564(1)	564(1)	sh, s
(PO$_4$)$^{3-}$	ν_2 out-of-plane bending (O-P-O)	472(1)	471(1)	b, w
(CaO$_5$OH)$^{9-}$ [5]	lattice mode (Ca-OH)	335(1)	-	b, w
(CaO$_9$)$^{16-}$; (CaO$_5$OH)$^{9-}$	lattice mode (Ca-O)	304(1)	-	sh, w
(CaO$_9$)$^{16-}$; (CaO$_5$OH)$^{9-}$	lattice mode (Ca-O)	291(1)	-	sh, w
(CaO$_9$)$^{16-}$; (CaO$_5$OH)$^{9-}$	lattice mode (Ca-O)	270(1)	-	sh, w
(PO$_4$)$^{3-}$	ν_2' out-of-plane bending (O-P-O)	261(1)	-	b, w

(1) assumptions according to Badiel & Berry (1966), Bhatnagar (1968), LeGeros et al. (1970) and Fowler (1973); (2) s: strong, m: medium, w: weak, vs: very strong, sh: sharp, b: broad, shd: shoulder; (3) due to the adsorbed water; (4) bands due to the (CO$_3$)$^{2-}$ groups in apatite "(CaOH)"; (5) also assigned to a composite mode ν_3 – ν_4 (Bhatnagar 1968). Analyzed samples: D 15 A, D 40 B, D 42 A, D 58 B, D 131 A (IR) and D 18 A, D 46 A, D 48 A, D 173 A, D 200, D 201 B, D 301 C, D 310 B, D 313 A (FTIR).

molecular H$_2$O (Table 6). This may be due to the very fine-grained nature of our samples, whose specific surfaces are large enough to adsorb molecules of H$_2$O, or to the presence of molecular H$_2$O in the structure of the analyzed samples, if they are Ca-deficient. In fact, in Ca-deficient apatite-(CaOH), the protonation of some of the phosphate groups respects a charge-balance scheme [Ca^{2+} + (OH)$^-$ + (PO$_4$)$^{3-}$] $\rightleftarrows$ (HPO$_4$)$^{2-}$, resulting in vacancies in both Ca and hydroxyl sites. It is very likely that molecules of H$_2$O occupy some of the vacated hydroxyl sites, being present in the c^*-axis anion channels (Ivanova et al. 2001, Elliott 2002). The presence in our samples of bands due to molecular H$_2$O also agrees with the result of the wet-chemical analysis (Table 4).

(2) A band at ~3570 cm^{-1} is characteristic for the O–H stretching involving the hydroxyl group in apatite. According to the bond distance – frequency correlation of Libowitzky (1999) [ν_{O-H} = 3632 – 1.79 × 10^6• exp (–d/0.2146)], this frequency corresponds to a H...O distance of 0.957 Å, identical to that determined by Kay et al. (1964) for the O–H distance in the (OH) group of apatite-(CaOH). The corresponding librations are expressed by the band at 635 cm^{-1}.

(3) The splitting into two fundamental vibrations of the antisymmetric stretching of the carbonate group (bands at ~1456 and ~1420 cm^{-1}) agrees with the assumption that carbonate groups in our samples

occupy two structural positions (*e.g.*, Brophy & Nash 1968, Elliott 2002). The corresponding bending seems unsplit, marked by a band centered at ~873 cm^{-1}. In fact, the out-of-plane bending of carbonate must in turn be doubly degenerate owing to the presence of carbonate groups in two different structural environments, but a second band, normally recorded at ~880 cm^{-1}, is too weak to be observed (Elliott 2002). The ν_2 bending of carbonate obscures the P–O(H) symmetric stretching of the $(HPO_4)^{2-}$ groups, which must be expressed by a band centered at practically the same wavenumber (Berry 1967, Ishikawa *et al.* 1993). In turn, the (P)O–H antisymmetric stretching at ~2930 cm^{-1} is too weak to be observed as a shoulder of the broad band due to the stretching of the molecular H_2O.

(4) The tetrahedral phosphate anion seems to generate nine vibrational modes, whose corresponding bands are tentatively assigned in Table 6. It is unclear if the band at ~335 cm^{-1} corresponds to the ν_2 out-of-plane bending of the phosphate group (Baddiel & Berry 1966, Bhatnagar 1968) or is due to a Ca–OH motion (Fowler 1973), or if the band at ~261 cm^{-1} corresponds to the ν_2' out-of-plane bending of the phosphate group (Baddiel & Berry 1966, Bhatnagar 1968) or to a lattice mode (Fowler 1973), but the band multiplicity ($3\nu_3 + 1\nu_1 + 3\nu_4 + 2\nu_2$) is consistent with a C_6 point symmetry of the phosphate anion.

(5) Shoulders toward the high-wavenumber side of the large complexes of bands at 900–1200 cm^{-1} (the phosphate-stretching region) and 500–650 cm^{-1} (phosphate in-plane bending region), potentially due to the presence of sulfate groups in the structure, are too poorly resolved. Such bands were reported by Baumer *et al.* (1990) in sulfate-substituted fluorapatite samples, but are not evident in our case.
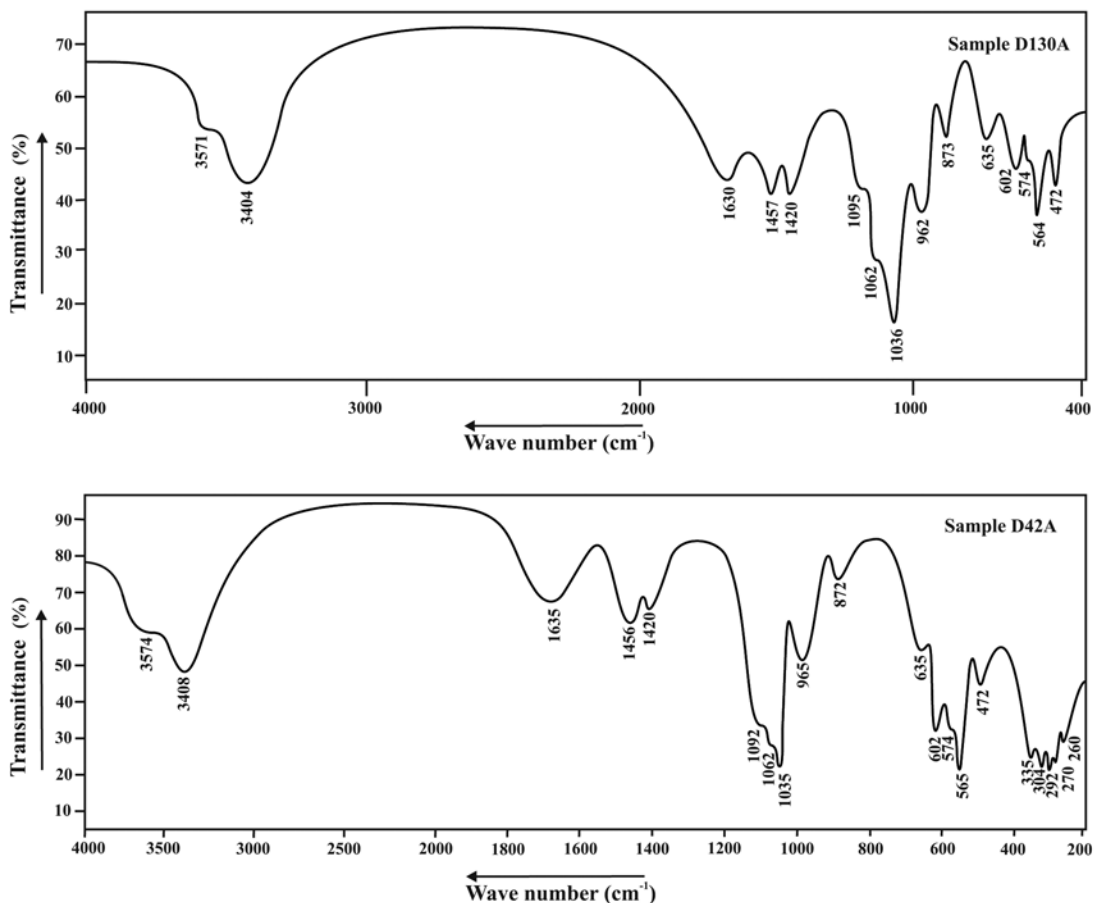
Fig. 5.   Infrared spectra of two selected samples of apatite-(CaOH) from Cioclovina: FTIR spectrum (top) and IR spectrum (bottom).

Genetic Considerations

Textual evidence, as well as parallels with other similar deposits, show that apatite-(CaOH) from Cioclovina formed by two complementary processes, namely: (1) by authigenesis, as reaction products between carbonate (basement, boulders or moonmilk flows) and acid solutions derived from guano, and (2) by sedimentation followed by diagenesis of organic relics such as bones, teeth and other tissues, in one of the richest deposits of fossil fragments in Europe. Both authigenic and biogenic apatite-(CaOH) from Cioclovina are carbonate- and sulfate-bearing and Ca-deficient. The lack of major physical, crystallographic and chemical differences between the two kinds of apatite-(CaOH) from Cioclovina is an argument in favor of re-equilibration during diagenesis.

An XRD analysis coupled with SEM–EDS, as well as textural evidence, show that the authigenic apatite-(CaOH) had a gel-like, X-ray-amorphous precursor. The nature of this precursor ("ACP phase") is unclear, but we presume that it is identical to that observed during the growth of synthetic apatite-(CaOH), having a composition like $Ca_3(PO_4)_2 \cdot nH_2O$ (Francis & Webb 1971, Abbona & Franchini-Angela 1990). This phase is unstable and normally transforms into the more stable phases octacalcium phosphate $[Ca_4H(PO_4)_3 \cdot 2.5H_2O]$ and apatite-(CaOH) (Abbona & Franchini-Angela 1990). As shown by Christoffersen *et al.* (1990), the octacalcium phosphate is the intermediate phase in the formation of apatite-(CaOH) *via* heterogeneous nucleation at increased supersaturation, which could explain the presence at Cioclovina of the spherical aggregates of densely matted material apparently crystallized from gels. The authigenic crystallization of apatite-(CaOH) by direct precipitation, as well as the recrystallization of biogenic fragments during diagenesis, were controlled by values of pH higher than 6.93 (Elliott *et al.* 1959) or 6.2 (Simpson 1964), this pH value essentially depending on the saturation of the mother solution. At low ranges of pH, the calcium phosphate expected to precipitate is brushite (Elliott *et al.* 1959, Simpson 1964). As proved by the frequency of the inclusions of quartz and illite in apatite-(CaOH) aggregates, the nucleation of Ca phosphates and the subsequent growth of apatite-(CaOH) seed crystals were stimulated by the pre-existence of silicate nuclei.

The contents of REE + Y reported previously (Table 3) are in the range of 2.95 to 47.11 ppm (average 12.79 ppm), even lower than those recorded by us in ten selected samples of carbonates from the limestone support and from the solidified flows of moonmilk on the walls, which range from 21.00 to 34.19 ppm (average 25.28 ppm). The classical hypothesis of the formation of authigenic apatite-(CaOH) by direct reaction between the phosphate solutions derived from the guano mass and the carbonates in the cave is consequently fully confirmed.

The coexistence of apatite-(CaOH) with brushite is essentially a function of the local variations of pH. The action of magnesium as local inhibitor of apatite-(CaOH) crystallization (Abbona & Franchini-Angela 1990) is excluded since the magnesium phosphates are lacking in the fossil guano, and in the surrounding limestones the level of concentration of magnesium is low. The inhibitor of the crystal growth of apatite-(CaOH) must in fact be the local excess of carbonate ions resulting from the breakdown of carbonates due to the acidity of solutions derived from the guano mass. This may explain the extensive development of brushite in the vicinity of the gel-like aggregates of Ca phosphate preceding apatite-(CaOH). The excess of sulfate in the system and the low values of pH (up to 5.5) destabilize both brushite and apatite-(CaOH), favoring the crystallization of ardealite or even gypsum (Rinaudo & Abbona 1988). This environment could explain the local occurrence of sprays and crusts of ardealite and gypsum directly on apatite-(CaOH).

References

Abbona, F. & Franchini-Angela, M. (1990): Crystallization of calcium and magnesium phosphates from solutions of low concentration. *J. Crystal Growth* **104**, 661-671.

ALBERIUS-HENNING, P., LANDA-CANOVAS, A., LARSSON, A.-K. & LIDIN, S. (1999): Elucidation of the crystal structure of oxyapatite by high-resolution electron microscopy. *Acta Crystallogr.* **B 55**, 170-176.

APPLEMAN, D.E. & EVANS, H.T., JR. (1973): Indexing and least-squares refinement of powder diffraction data. *U.S. Geol. Surv., Comput. Contrib.* **20** (NTIS Doc. **PB-216**).

BADDIEL, C.B. & BERRY, E.E. (1966): Spectra structure correlations in hydroxy and fluorapatite. *Spectrochim. Acta* **22**, 1407-1416.

BALENZANO, F., DELL'ANNA, L. & DI PIERO, M. (1974): Ricerche mineralogiche su alcuni fosfati rinvenuti nelle grotte di Castellana (Bari): strengite aluminifera, vivianite, taranakite, brushite e idrossiapatite. *Rend. Soc. Ital. Mineral. Petrogr.* **30**, 543-573.

BAUMER, A., CARUBA, R. & GANTEAUME, M. (1990): Carbonate-fluorapatite: mise en évidence de la substitution $2PO_4^{3-} \rightarrow SiO_4^{4-} + SO_4^{2-}$ par spectrométrie infrarouge. *Eur. J. Mineral.* **2**, 297-304.

BENOIT, P.H. (1987): Adaptation to microcomputer of the Appleman–Evans program for indexing and least-squares refinement of powder-diffraction data for unit-cell dimensions. *Am. Mineral.* **72**, 1018-1019.

BERRY, E.E. (1967): The structure and composition of some calcium-deficient apatites. *J. Inorg. Nucl. Chem.* **29**, 317-327.

BHATNAGAR, V.M. (1968): Infrared spectra of hydroxyapatite and fluorapatite. *Bull. Soc. Chim. France*, 1771-1773.

BROPHY, G.P. & NASH, T.J. (1968): Compositional, infrared and X-ray analysis of fossil bone. *Am. Mineral.* **53**, 445-454.

BRUNET, F., ALLAN, D.R., REDFERN, A.T.S., ANGEL, R.J., MILETICH, R., REICHMANN, H.J., SERGENT, J. & HANFLAND, M. (1999): Compressibility and thermal expansivity of synthetic apatites, $Ca_5(PO_4)_3X$ with X = OH, F and Cl. *Eur. J. Mineral.* **11**, 1023-1035.

BURKE, E.A.J. (2008): Tidying up mineral names: an IMA–CNMNC scheme for suffixes, hyphens and diacritical marks. *Mineral. Rec.* **39**, 131-135.

CHRISTOFFERSEN, M.R., CHRISTOFFERSEN, M.R. & KIBALCZYC, W. (1990): Apparent solubilities of two amorphous calcium phosphates and of octacalcium phosphate in the temperature range 30–42°C. *J. Crystal Growth* **106**, 349-354.

CONSTANTINESCU, E., MARINCEA, Ş. & CRĂCIUN, C. (1999): Crandallite in the phosphate association from Cioclovina cave (Şureanu Mts., Romania). *In* Scientific works by Emil Constantinescu. Mineralogy in the System of Earth Sciences. Imperial College Press, London, U.K. (1-5).

DIACONU, G. & MEDEŞAN, A. (1975): Spéléothèmes de dahllite dans la grotte "Peştera Muierii", Baia de Fier – Roumanie. *Trav. Inst. Spéol. "Emile Racovitza"* **14**, 149-156.

DOROZHKIN, S.V. & EPPLE M. (2002): Die biologische und medizinische Bedeutung von Calciumphosphaten. *Angew. Chem.* **114**, 3260-3277.

DUMITRAŞ D.G., MARINCEA, Ş. & FRANSOLET, A.M. (2004): Brushite in the bat guano deposit from the "dry" Cioclovina Cave (Şureanu Mountains, Romania). *Neues Jahrb. Mineral., Monatsh.*, 45-64.

ELLIOT, J.S., SHARP, R.F. & LEWIS, L. (1959): The effect of the molar Ca/P ratio upon the crystallization of brushite and apatite. *J. Phys. Chem.* **63**, 725-726.

ELLIOTT, J.C. (1994): *Structure and Chemistry of the Apatites and the Other Calcium Orthophosphates*. Elsevier, Amsterdam, The Netherlands.

ELLIOTT, J.C. (2002): Calcium phosphate biominerals. *In* Phosphates – Geochemical, Geobiological and Materials Importance (M.L. Kohn, J. Rakovan & J.M. Hughes, eds.). *Rev. Mineral. Geochem.* **48**, 427-454.

FIORE, S. & LAVIANO, R. (1991): Brushite, hydroxylapatite, and taranakite from Apulian caves (southern Italy): new mineralogical data. *Am. Mineral.* **76**, 1722-1727.

FOWLER, B.O. (1973): Infrared studies of apatites. I. Vibrational assignments for calcium, strontium and barium hydroxyapatites utilizing isotopic substitution. *Inorg. Chem.* **13**, 194-207.

FRANCIS, M.D. & WEBB, N.C. (1971): Hydroxyapatite formation from a hydrated calcium monohydrogen phosphate precursor. *Calc. Tiss. Res.* **6**, 335-342.

HUGHES, J.M., CAMERON, M. & CROWLEY, K.D. (1989): Structural variations in natural F, OH and Cl apatites. *Am. Mineral.* **74**, 870-876.

IOSOF, V. & NEACŞU, V. (1980): Analysis of silicate rocks by atomic absorption spectrometry. *Rev. Roum. Chim.* **25**, 589-597.

ISHIKAWA, K., DUCHEYNE, P. & RADIN, S. (1993): Determination of the Ca/P ratio in calcium-deficient hydroxyapatite using X-ray diffraction analysis. *J. Mater. Sci., Mater. Med.* **4**, 165-168.

IVANOVA, T.I., FRANK-KAMENETSKAYA O.V., KALTSOV, V. & UGOLKOV, L. (2001): Crystal structure of calcium-deficient carbonated hydroxylapatite. Thermal decomposition. *J. Solid State Chem.* **160**, 340-349.

KAY, M.I., YOUNG, R.A. & POSNER, A.S. (1964): Crystal structure of hydroxylapatite. *Nature* **204**, 1050-1052.

LEGEROS, R.Z., LEGEROS, J.P., TRAUTZ, O.R. & KLEIN, E. (1970): Spectral properties of carbonate in carbonate-containing apatites. *Develop. Appl. Spectrosc.* **7 B**, 3-12.

LIBOWITZKY, E. (1999): Correlation of O–H stretching frequencies and O–H...O hydrogen bond lengths in minerals. *Monatsh. Chem.* **130**, 1047-1059.

MANDARINO, J.A. (1981): The Gladstone–Dale relationship. IV. The compatibility concept and its application. *Can. Mineral.* **19**, 441-450.

MARINCEA, Ş. & DUMITRAŞ, D. (2003): The occurrence of taranakite in the "dry" Cioclovina Cave (Sureanu Mountains, Romania). *Neues Jahrb. Mineral., Monatsh.*, 127-144.

MARINCEA, Ş. & DUMITRAŞ, D. (2005): First reported sedimentary occurrence of berlinite (AlPO₄) in phosphate-bearing sediments from Cioclovina Cave, Romania – Comment. *Am. Mineral.* **90**, 1203-1208.

MARINCEA, Ş., DUMITRAŞ, D. & GIBERT, R. (2002): Tinsleyite in the "dry" Cioclovina Cave (Sureanu Mountains, Romania): the second world occurrence. *Eur. J. Mineral.* **14**, 157-164.

MORTIER, A., LEMAITRE, J. & ROUXHET, P.G. (1989): Temperature-programmed characterization of synthetic calcium-deficient phosphate apatites. *Thermochim. Acta* **143**, 265-282.

NEWESELEY, H. (1963): Kristallchemische und micromorphologische Untersuchungen an Carbonat-Apatiten. *Monatsh. Chem.* **94**, 270-280.

ONAC, B.P., BREBAN, R., KEARNS, J. & TAMAS, T. (2002): Unusual minerals related to phosphate deposits in Cioclovina cave, Sureanu Mountains (Romania). *Theor. Appl. Karst.* **15**, 27-34.

ONAC, B.P., ETTINGER, K., KEARNS, J & BALASZ, I.I. (2005): A modern, guano-related occurrence of foggite, CaAl(PO₄)(OH)₂•H₂O and churchite-(Y), YPO₄•2H₂O in Cioclovina Cave, Romania. *Mineral. Petrol.* **85**, 291-302.

ONAC, B.P. & WHITE, W.B. (2003): First reported sedimentary occurrence of berlinite (AlPO₄) in phosphate-bearing sediments from Cioclovina cave, Romania. *Am. Mineral.* **88**, 1395-1397.

RINAUDO, C. & ABBONA, F. (1988): A contribution to the study of the crystal chemistry of calcium sulfate phosphate hydrate. *Mineral. Petrogr. Acta* **31**, 95-105.

SCHADLER, J. (1929): Mineralogische-petrographische Characteristik der Phosphat-Ablagerung in der Cioclovinahöhle bei Pui. *Pub. Muz. Hunedoara* **5**(27), 1-3.

SCHADLER, J. (1932): Ardealit, ein neues Mineral CaHPO₄•CaSO₄+4H₂O. *Zb. Mineral.* **A**, 40-41.

SHAPIRO, L. & BRANNOCK, W.W. (1962): Rapid analysis of silicate, carbonate and phosphate rocks. *U.S. Geol. Surv., Bull.* **1144-A** (A 14-15, A 49-51).

SIMPSON, D.R. (1964): The nature of alkali carbonate apatites. *Am. Mineral.* **49**, 363-376.

TOMUŞ, R.B. (1999): *The Karst Complex Ciclovina. The Basin 2063*. Proteus, Hunedoara, Romania (in Romanian).

TRUEMAN, C.N. & TUROSS, N. (2002): Trace elements in recent and fossil bone apatite. *In* Phosphates – Geochemical, Geobiological and Materials Importance (M.L. Kohn, J. Rakovan & J.M. Hughes, eds.). *Rev. Mineral. Geochem.* **48**, 489-522.